*J. Fluid Mech.* (1989), *vol.* 198, *pp.* 321–344
*Printed in Great Britain*



# Wavenumber spectra of short gravity waves

By M. L. BANNER†, IAN S. F. JONES‡ AND J. C. TRINDER§

†School of Mathematics, University of New South Wales, PO Box 1, Kensington, NSW 2033, Australia
‡RAN Research Laboratory, PO Box 706, Darlinghurst, NSW 2010, Australia.
§School of Surveying, University of New South Wales, PO Box 1, Kensington, NSW 2033, Australia

(Received 5 June 1986 and in revised form 14 June 1988)

The spectral balances involved in shaping the short gravity wave region of the ocean wave-height spectrum have been the subject of recent physical models. In terms of the wind friction velocity $u_*$, gravitational acceleration $g$ and local wavenumber $\boldsymbol{k}$, these models predict a wavenumber dependence of $k^{-\frac{7}{2}}$, where $k = |\boldsymbol{k}|$, and a linear dependence on $u_*$ for the equilibrium range of gravity waves above the spectral peak. In this paper we present the results of an experimental determination of the wavenumber spectrum for the wavelength range of 0.2–1.6 m, based on stereo-photogrammetric determinations from an oil platform under open ocean conditions.

From our observations, for this wavenumber range, the one-dimensional equilibrium wavenumber spectrum was determined as

$$\phi(k_i) \sim \left(\frac{u_*^2 k_i}{g}\right)^{\gamma} k_i^{-3} \quad (i = 1, 2, \quad \boldsymbol{k} = (k_1, k_2)),$$

where $\gamma = 0.09 \pm 0.09$ at the 95% confidence level. These limits embrace wind-independent approximations to the observed one-dimensional and two-dimensional wavenumber spectra of the form

$$\phi(k_i) \sim B\, k_i^{-3} \quad (i = 1, 2),$$

and

$$\psi(\boldsymbol{k}) \sim A k^{-4},$$

respectively, with $B \sim 10^{-4}$ and $A \sim 0.3 \times 10^{-4}$ for $(u_*^2 k_i/g) = 10^{-2}$, and $k = |\boldsymbol{k}|$ is expressed in cycles/metre.

The present findings do not support the wavenumber dependence predicted by the recent models in this wavenumber range and are at variance with their predicted dependence on the friction velocity. However, our observations are generally consistent with the radar reflectivity dependence on wind direction and wind speed under Bragg scattering conditions within our wavenumber range. The experimental observations also point out the potentially important role of wave-breaking of longer wave components in influencing the spectral levels of short gravity wave components.

## 1. Introduction

Oceanic motions are driven by air–sea interchanges and interfacial waves play an essential part in this process. The very short waves form the basis for much of the future development of remote sensing of the ocean surface by satellites. Satellite radars for monitoring ocean waves and wind stress (e.g. SEASAT) have shown

considerable promise of being able to determine winds and waves associated with severe storms on a timescale sufficient to provide warnings for marine operations, such as oil and gas platform evacuation.

Accurate determinations of sea surface statistics, and in particular elevation wavenumber spectra for short waves are needed to answer a number of important questions of fundamental and technological interest. Little is known about the directional wavenumber spectral distribution of short waves, particularly as they are modulated by underlying ocean swell components under wind forcing. This information is fundamental in calculating acoustic and electromagnetic backscattering from the sea surface for low roughness (no shadowing) conditions. Most of the available wavenumber spectral information has been inferred from backscattered microwave data on the basis of the assumption that Bragg resonant backscattering is the dominant reflection mechanism (Valenzuela 1985). The present investigation is concerned with a more direct determination of the short ocean gravity wind wave regime in terms of wavenumber spectra: a motivational aspect of this work concerns reconciliation of the observed sea surface microstructure with that inferred from the microwave observations. However, the main concern of this study is an examination of the physical processes which determine the wavenumber spectrum of very short ocean waves, in terms of the relative importance of the source functions arising from wind input, nonlinear spectral transfer and dissipation. For short gravity waves under open ocean conditions, these terms remain to be determined. However, useful inferences can be made from the form of the surface elevation wavenumber spectrum for this wavenumber range.

Historically, on account of the relative ease of measurement, most previous direct spectral determinations of the short ocean gravity wave regime have been in terms of frequency spectra using capacitance wire probes. In the frequency band 1.5–10 Hz, corresponding to wavelengths of 0.7–0.016 m, Kondo, Fujinawa & Naito (1972) found the power spectral density depended on $f^{-n}$ with $n$ between 3 and 3.3. For $u_{10.5} = 8$ m/s and a fetch of 2 km, Mitsuyasu (1977) found $f^{-5}$ for $0.6 < f < 4$ Hz, and $f^{-4}$ for $4 < f < 15$ Hz. Stolte (1984) reported similar findings with exponents of 4.2 for $U_{19.5} = 3.3$ m/s, 3.9 for $U_{19.5} = 8.9$ m/s, ? ɔ for $U_{19.5} = 14.6$ m/s and 3.3 for $U_{19.5} = 19.0$ m/s. This is weaker dependence on frequency than the traditionally adopted prescription of Phillips' $f^{-5}$ equilibrium frequency spectrum (Phillips 1958). Ocean wave-slope frequency spectra have been reported by Tang & Shemdin (1983), using an optical device attached to a wave follower. They showed that the most energetic frequency components of upwind–downwind slope occurred near the spectral peak in the displacement spectrum. Their study covered the wind speed range 3.0 m/s to 11.3 m/s.

Of central concern with this type of measurement is the intrinsic difficulty of transforming either class of frequency spectra directly to wavenumber spectra because of Doppler shifting of the short-wave components by the underlying longer-wavelength components from possibly different directions. For example, an ocean wave of period 7 s only needs a slope of 0.05 to provide the necessary Doppler shift for a short wave of 0.1 m wavelength to have zero apparent frequency in the trough region. In practice, with the possibility of multiple directional swell components and of locally varying short-wave directional energy distributions over the scale of the underlying swells, transformation of the local frequency spectra into wavenumber (magnitude) spectra is not straightforward. Kitaigorodskii, Krasitskii & Zaslavskii (1975) contains a detailed theoretical discussion of the underlying issues while various investigators (e.g. Evans & Shemdin 1980; Stolte 1984; Richter & Rosenthal

1986; Atakturk & Katsaros 1987) present attempts at the transformation of field data.

While there have been a number of determinations of frequency spectra for short ocean waves, there have been far fewer wavenumber determinations owing to the need for a very large number of simultaneous elevation determinations with high horizontal and vertical resolution. These requirements effectively preclude conventional point-probe arrays in the context of open ocean measurements. Most previous studies reporting wavenumber data for short ocean waves have been based on an assumed proportionality between the wave slope and the local image grey scale on photographic images of the sea surface. This technique is premised on uniform sky illuminance. The photographic image is illuminated in a coherent optical bench apparatus to produce a diffraction pattern which is the two-dimensional wavenumber spectrum of the image intensity. This is claimed to be proportional to the two-dimensional slope spectrum from which the two-dimensional height spectrum is then readily derived. This method is described by Stillwell (1969) and by Stillwell & Pilon (1974) and has formed the basis of more recent studies by Lubard *et al.* (1980) and Gotwols & Irani (1980). Lubard *et al.* (1980) reported initial results of a comparison between this optical method and a wave-follower driven laser wave-slope detector, similar to the device used by Tang & Shemdin (1983). Their data showed certain systematic differences between the two methods and also revealed sample spectra which showed significant deviation from the equilibrium spectra commonly assumed (e.g. see Phillips 1977*a*, §4.5).

The optical method used in these single photograph studies has the advantage of simplicity of processing to obtain the wavenumber slope spectra. However, the assumptions behind the method have not been checked exhaustively, particularly for the short-wave scales. Also, this method lacks an absolute calibration in terms of physical sea surface heights or slopes and must be normalized using auxiliary measurements of either of the quantities. In view of the restrictions to uniform sky illuminance conditions, the lack of an absolute calibration and the systematic discrepancies noted by Sugimori (1975) and by Lubard *et al.* (1980), it is clearly desirable to attempt to make these determinations using more direct methods, if feasible. The well-established technique of stereophotogrammetry (e.g. Pierson 1962; Dobson 1970; Sugimori 1975; Holthuijsen 1983) offers the potential to provide absolute reconstructions of the sea surface topography with less restrictive assumptions on the ambient lighting conditions, though at the expense of increased data reduction effort.

In this paper we report the results of an investigation aimed at determining accurately the wavenumber spectral characteristics of the short gravity wave regime of the sea surface elevation, using stereophotogrammetric techniques. Following a discussion of the theoretical background in §2 and a detailed description of the experimental procedures in §3 and data analysis methodology in §4, results are presented for directional and one-dimensional wavenumber spectra obtained for a range of typical open ocean conditions. These results are reviewed in the context of models for the wavenumber spectrum due to Phillips (1958) and with its recent revisions (Kitaigorodskii 1983; Phillips 1985). In terms of physical aspects, the results obtained here provide a detailed account of the mean characteristics of the wavenumber spectrum of very short gravity waves over a significant range of sea states. Although it is clearly a very significant aspect of this problem, a detailed examination of the modulational properties of the short-wave spectra is beyond the scope of the present contribution and is left to the future.

## 2. Theoretical background

The dynamical balances which determine the spectral dependence for scales much shorter than the spectral peak have been the subject of considerable observational and theoretical investigation. A lucid discussion on this topic is presented by Phillips (1985, §2) to which the reader is referred for a comprehensive review. However, in brief, the original hypothesis proposed by Phillips (1958) envisaged an equilibrium form determined primarily by dissipation though wave breaking which imposed a fixed upper limit on the spectral level, (otherwise known as 'hard-limiting'), independent of the wind strength. This model yielded the asymptotic form,

$$\psi(\boldsymbol{k}) = \alpha k^{-4} f(\theta),$$

for the two-dimensional wavenumber spectrum, $\psi(\boldsymbol{k})$, of the surface elevation. (The wavenumber vector $(k_1, k_2)$ and its polar form $(k, \theta)$ are used interchangeably here.) In the light of improved measurements of ocean wave frequency spectra, various investigators (e.g. Toba 1973; Kawai, Okuda & Toba 1977; Forristall 1981; Kahma 1981; Donelan, Hamilton & Hui 1985) have reported frequency spectra of the form

$$F(\sigma) \sim \sigma^{-4}$$

for frequencies $\sigma$ in the gravity range up to about three times the spectral peak frequency. Donelan *et al.* (1985) reported an approximately linear dependence of the constant of proportionality on the effective windspeed in the direction of wave propagation. Forristall (1981) and Kahma (1981) also found a linear dependence on the wind speed or friction velocity $u_*$ for this spectral region. These observations appear to have motivated Kitaigorodskii (1983) and more recently Phillips (1985) to propose revised equilibrium spectral balances in which wind input $S_{\mathrm{W}}$, nonlinear spectral transfer $S_{\mathrm{NL}}$ and dissipation by processes such as wave breaking $S_{\mathrm{DISS}}$ assume different levels of relative importance in determining the 'equilibrium' spectral form for the short gravity-wave range of the spectrum.

Kitaigorodskii (1983) proposed an equilibrium gravity wave subrange in which $S_{\mathrm{W}}$ is concentrated near the spectral peak with the dissipation $S_{\mathrm{DISS}}$ concentrated at the high wavenumber regime. The equilibrium range is envisaged as determined by the spectral energy flux determined by the wind energy input rate near the spectral peak, with local wind input, spectral flux divergence and dissipation playing a negligible role. In reviewing this model, Phillips (1985, §2) questioned the basic assumption of negligible wind input within the equilibrium range and postulated an alternate balance which is described conveniently in terms of the action spectral density $\psi(\boldsymbol{k})/\sigma$ (see Phillips 1977*b* for a detailed exposition). Komen, Hasselmann & Hasselmann (1984) also examined the Kitaigorodskii model and concluded that the proposed localization of $S_{\mathrm{W}}$ and $S_{\mathrm{DISS}}$ produced too rapid growth of the spectrum near its peak and failure of the spectrum to equilibrate.

For the equilibrium subrange of wavenumbers,

$$S_{\mathrm{W}} + S_{\mathrm{NL}} + S_{\mathrm{DISS}} = 0, \tag{2.1}$$

where $S_{\mathrm{W}}$ is the wind input rate of spectral action density, $S_{\mathrm{NL}}$ is the nonlinear spectral transfer rate, shifting spectral action density between different wavenumber components without changing the total spectral action and $S_{\mathrm{DISS}}$ is the rate of loss of spectral action density due to wave breaking and viscous effects.

Appropriate to the postulated equilibrium range, Phillips (1985, §2) suggested the following forms for the three terms.

$$S_{\mathrm{W}} = m \cos^{2p}\theta g\left(\frac{u_*}{c}\right)^2 \psi(\boldsymbol{k}),$$

$$S_{\mathrm{NL}} \sim g k^8 \psi^3(\boldsymbol{k}),$$

$$S_{\mathrm{DISS}} = g k^{-4} F(k^4 \psi(\boldsymbol{k})),$$

where $p$ and $m$ are empirical constants, $c$ is the phase speed, and where little is known about the functional form of the dissipation term. All three terms assume the rate of change of action spectral density can be expressed in terms of the local wavenumber and does not depend on much shorter or longer wavenumber components such as underlying swell. Dimensional reasoning can be used to find a form for $\psi(\boldsymbol{k})$ under the basic assumption that each of the above terms is comparable in magnitude in pairwise combinations, for which the following balances hold:

(*a*) $$S_{\mathrm{NL}} \sim S_{\mathrm{DISS}},$$

$$g k^8 \psi^3(\boldsymbol{k}) \sim g k^{-4} F\{k^4 \psi(\boldsymbol{k})\}.$$

If only power law dependence for $F$ is assumed, i.e.

$$g k^8 \psi^3(\boldsymbol{k}) \sim g k^{-4} \{k^4 \psi(\boldsymbol{k})\}^n,$$

then it is easily seen that

$$\psi(\boldsymbol{k}) \sim k^{-4}, \tag{2.2}$$

(except when $n = 3$, for which $\psi(\boldsymbol{k})$ is indeterminate based on this balance). This is the spectral dependence on wavenumber magnitude proposed originally by Phillips (1958), but the underlying balance is very different.

(*b*) $$S_{\mathrm{NL}} \sim S_{\mathrm{W}}$$

$$g k^8 \psi^3(\boldsymbol{k}) \sim g \cos^{2p}\theta \left(\frac{u_*}{c}\right)^2 \psi(\boldsymbol{k}),$$

with $$\psi(\boldsymbol{k}) \sim u_* g^{-\frac{1}{2}} k^{-\frac{7}{2}},$$

in which the angular dependence $\theta$ between the wind and wave component direction has been suppressed and the free gravity-wave dispersion relation $\sigma^2 = gk$ has been used. This is the spectral dependence proposed by Phillips (1985).

(*c*) $$S_{\mathrm{W}} \sim S_{\mathrm{DISS}},$$

Here $$\frac{u_*^2}{c^2} k^4 \psi(\boldsymbol{k}) \sim \{k^4 \psi(\boldsymbol{k})\}^n,$$

giving $$\psi(\boldsymbol{k}) \sim \left(\frac{u_*}{c}\right)^{\frac{2}{n-1}} k^{4\left(\frac{1-n}{n-1}\right)} \quad \text{for } n \neq 1.$$

This balance allows a range of wavenumber dependences all of the form

$$\psi(\boldsymbol{k}) \sim \left(\frac{u_*^2 k}{g}\right)^{\gamma} k^{-4}. \tag{2.3}$$

where $\gamma$ is a parameter. The case when $n \to \infty$ corresponds to the physical balance underlying Phillips (1958) equilibrium form for which $S_{\mathrm{DISS}}$ is implicitly assumed to be a very rapidly increasing function of $\psi(\boldsymbol{k})$, effectively damping any growth of $\psi(\boldsymbol{k})$ above its equilibrium ('hard') limit.

It also is of interest to note the differences in the form of the dissipation source term corresponding to Phillips (1985) equilibrium spectral model with the form proposed by Hasselmann (1974). On the basis of the balance proposed by Phillips (1985),

$$S_{\mathrm{DISS}} \sim g k^8 \psi^3(\boldsymbol{k}).$$

The explicit cubic dependence on $\psi(\boldsymbol{k})$ reflects the strongly nonlinear behaviour of the dissipation envisaged by Phillips. In contrast, Hasselmann (1974) argued that the dissipation is quasi-linear in $\psi(\boldsymbol{k})$ for dissipative processes which are weak-in-the-mean, where

$$S_{\mathrm{DISS}} \sim g \Gamma(\boldsymbol{k}) \psi(\boldsymbol{k}).$$

$\Gamma(\boldsymbol{k})$ depends not only on the local wavenumber but on integral properties of the wave spectrum, such as the average wave steepness. A possibility is that these proposed forms may be applicable to different regions of the wave spectrum.

In any event, with the obvious uncertainty in the relative weightings of the spectral source terms in (2.1), we note that on the basis of simple dimensional reasoning, any power law equilibrium spectral form for our spectral region of interest which is assumed to depend only on $u_*$, $g$ and $k$ must be of the form

$$\psi(\boldsymbol{k}) \sim \left(\frac{u_*^2 k}{g}\right)^{\gamma} k^{-4}. \tag{2.4}$$

The extent to which our observations conform to this relationship is analysed below.

## 3. Procedure

The measurements were made at sea from the ESSO/BHP platform Barracouta in a water depth of 47 m. This platform, located at longitude 147° 40′ E and latitude 38° 18′ S, 20 km from shore, was fitted with a 16 m boom so that the sea was sampled clear of disturbance induced by the platform structure. Wills (1984) found in wind-tunnel models of an offshore structure that flow distortion was small at these distances. The camera configuration was designed to provide a 2 m × 2 m overlap area on the sea surface for subsequent stereophotogrammetric analysis. The stereophotographic data was recorded with synchronized 35 mm cameras (Olympus OM-1N) and the techniques described by Karara & Abdel-Aziz (1974) used to calibrate the unknown properties of the camera lenses. The three dimensions of an object can be determined from the coordinates of corresponding image points on two overlapping photographs provided the camera positions and tilts are known.

The relative values of the base $B$, the distance between the camera stations and the height $H$ of the cameras above the object being measured (see figure 1), will affect the accuracy of measurement of height coordinates. For a good geometric configuration the $B/H$ or base/height ratio should approach 0.5. For 35 mm format cameras, lenses with focal lengths in excess of 50 mm are unsatisfactory because the $B/H$ is too small; for the 50 mm focal length lenses used to gather the data reported here, the $B/H$ ratio was approximately 0.3, while for the 35 mm focal length lenses the $B/H$

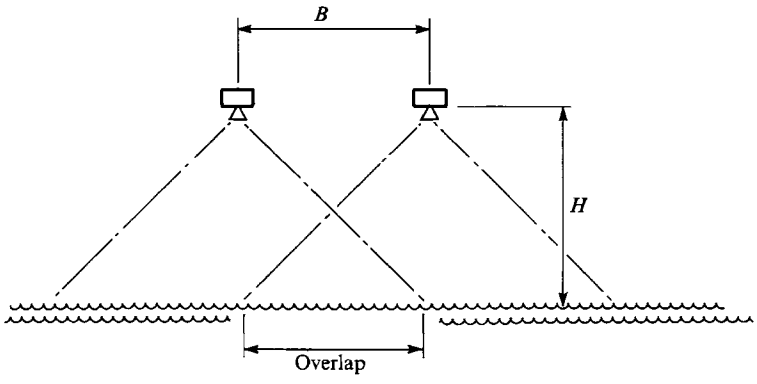


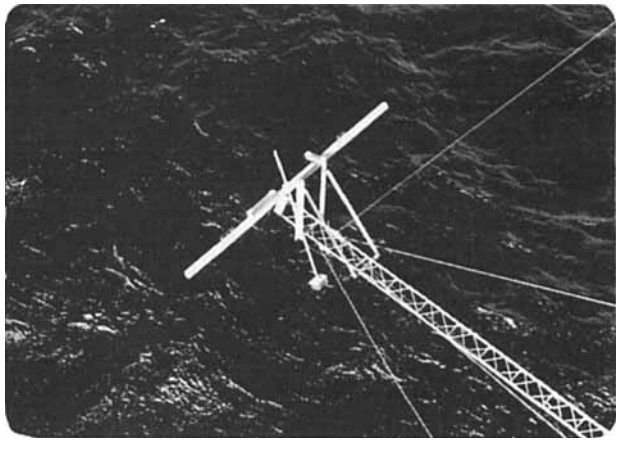

FIGURE 1. Stereoscopic camera configuration.

was about 0.4. For this project the cameras were mounted 2 m or 3.2 m apart on a rigid beam and were deployed at a mean height of 5–10 m above the sea surface, providing the desired approximately 2 m × 2 m overlap area at a $B/H > 0.3$. Figure 1 also provides an *in situ* view of the camera boom.

Synchronization of the cameras was found to be better than $\frac{1}{500}$ s at $\frac{1}{500}$ s exposure setting. This was determined by photographing a spinning disk with an engraved radial line. Knowing the rotation rate and the exposure duration enabled conversion of an angular error to a relative temporal lag. A repetition (firing) rate for the cameras was chosen to be 2 frames per second. It was anticipated that this would provide suitable sampling for 5–10 s periods typical of Bass Strait waves.

The film used to record the primary data was chosen on the basis of certain somewhat conflicting requirements. The final choice was necessarily a compromise. The criteria for the recording film were:

(*a*) stable (polyester) base to eliminate changes in geometry due to stretching of the film during processing;

(*b*) moderate contrast to optimize the stereophotogrammetric viewability of the local sea surface topography (an intrinsically low-contrast surface);

(*c*) high ASA rating, to allow small-to-moderate apertures at the fast shutter

speed of $\frac{1}{500}$ s, needed to ensure adequate depth of field for maintaining focus of the images.

After extensive testing, the final choice of film was Ilford Type 400-P4 which satisfied criteria (*a*) and (*b*) particularly well, but was only moderately fast (nominally 400 ASA) necessitating the use of excessively wide apertures. To reduce the apertures, the film rating was boosted to 1600 ASA using push-processing, which did not adversely affect the image quality under the actual data collection conditions.

Auxiliary measurements of the large-scale waves and the wind were also recorded. The surface elevation below the cameras was sensed by an acoustic travel time device which sampled the water height every 0.5 s. Also a Baylor wave gauge was located on the south western edge of the platform and this was used to determine average wave period and significant wave height. The magnitude and direction of the wind was recorded by the platform wind gauge, mounted 54 m above the mean sea level.

The test range of targets used to calibrate the cameras must be displaced in three coordinate directions for a solution of the parameters of the camera, that is principal point, focal length and the geometric distortions introduced by the lens. For the calibration of the camera lenses used in this study, 32 targets covered the overlap area of 2 photographs in an area of about 2 m × 1 m. Twenty-four targets were placed on the same plane, and 8 projected from the plane 0.8 m. The photography distance was 6 m, matching that of the intended photography. The positions of the targets were determined by metric camera photography, i.e. using a camera of known calibration and by field surveying methods to an accuracy of 0.5 mm. Photograph coordinates of the 2 calibration images of the test range were observed to an accuracy of approximately 3 μm on an analytical stereoplotter, which is a computer-assisted instrument enabling the simultaneous observation of photograph coordinates on the photography, and the real-time computation of the basic photogrammetric equations relating photograph and object space coordinates to determine the sea surface coordinates. Special close-range camera calibration software was used to determine the unknown camera calibration parameters, required as input data to the stereoplotter in the determination of the sea surface coordinates, as described below. For the calibration photography, the differences between the computed coordinates and the survey coordinates either locally or expressed as r.m.s. over the overlap region were very close to 1 mm in each of the three coordinate directions.

A complete solution of the photogrammetric equations requires knowledge of the camera station coordinates in an appropriate coordinate system, and also the camera tilts (i.e. angular rotations about three orthogonal axes, taken conveniently as joining the camera stations, the $x$-axis; parallel to the mean target plane, the $y$-axis; and normal to the target plane, the $z$-axis). The sea surface measurements, however, require only relative measurements of points, but the physical scale of the details must be correct. Scale is dependent on the distance between the two camera positions (the base), which is fixed during photography. This scaling was verified by the agreement between the photogrammetric and acoustic ranger determinations of sea surface height. An incorrect determination of the tilts will primarily result in introducing a small slope in the measured sea surface which will not significantly affect the relative measurements of coordinates. To facilitate stereoscopic observations, the rotations about the $z$-axis of each photograph were computed by the analytical plotter software. This computation eliminated the displacements parallel to the $y$-axis between corresponding image points during observations. Following the

orientation process, for each scene a uniform grid of three-dimensional points was observed stereoscopically over the sea surface in the stereo plotter, as described in the following section.

## 4. Data analysis

The photographic frames selected for processing were sampled over a $33 \times 33$ grid with a nominal ground spacing of 50 mm using both a pattern of east–west and north–south traverses. The mean elevation of each frame was determined from the stereogrammetric analysis and checked against the simultaneously recorded wave-height signal from the collocated acoustic time of flight device.

A two-dimensional transform $\mathrm{d}Z(k_1, k_2)$ of the sea surface elevation, $\eta(r_1, r_2)$ was defined as a generalized function by

$$\mathrm{d}Z(k_1, k_2) = \left(\frac{1}{2\pi}\right)^2 \int\int_{-\infty}^{\infty} \eta(r_1, r_2) \exp\left(\mathrm{i}k_1 r_1 + \mathrm{i}k_2 r_2\right) \mathrm{d}r_1 \, \mathrm{d}r_2,$$

and the one-dimensional transform $\mathrm{d}X(k_1, r_2)$ by

$$\mathrm{d}X(k_1, r_2) = \frac{1}{2\pi} \int_{-\infty}^{\infty} \eta(r_1, r_2) \exp\left(\mathrm{i}k_1 r_1\right) \mathrm{d}r_1,$$

with an analogous transform for the $k_2$ wavenumber.

The above transforms were approximated by the fast Fourier transform of the sea elevation at discrete horizontal separations. Since the present data series are short compared with the energetic low wavenumber components of the wave spectrum, the resulting low-order trends in the photographic records were suppressed by taking first differences of the sea surface height before performing the transform along the east–west lines, designated $\mathrm{d}Z_{\mathrm{E}}$, and taking first differences along the north–south lines, designated $\mathrm{d}Z_{\mathrm{N}}$. This form of prewhitening is equivalent to applying a high-pass filter to the power spectrum of the form

$$(2 - 2\cos 2\pi k_i \Delta r_i) \quad (i = 1, 2),$$

where $\Delta r_i$ in the spacing over which the first difference was computed. This effectively filtered out the low-wavenumber information (where most of the energy lies). To make this process definite for recolouring and to maintain a symmetry, we prescribed

$$\mathrm{d}Z(k_1 = 0, k_2) = \mathrm{d}Z(k_1, k_2 = 0) = 0.$$

Since $\mathrm{d}Z(k_1, k_2)$ or $\mathrm{d}X(k_1, r_2)$ are complex variables with phases that depend on the origin chosen for $r_1$ and $r_2$, the results are presented as power spectra. The two-dimensional spectrum was defined as

$$\psi(k_1, k_2) = \frac{1}{n} \sum^{n} \left| \lim_{\delta k \to 0} \frac{\mathrm{d}Z_{\mathrm{E}}(k_1, k_2) \, \mathrm{d}Z_{\mathrm{N}}^{*}(k_1, k_2)}{\delta k_1 \, \delta k_2} \right| \tag{4.1}$$

where $1/n \sum^n$ implies the average over a number $n$ of photographic frames and $||$ denotes the modulus. Using the Fourier transforms of the prewhitened series the products of the transforms were recoloured.

For the one-dimensional spectra, which must be symmetric in wavenumber, the products of the transforms were doubled so that

$$\phi(k_1) = \frac{2}{n} \sum_{r_2} \lim_{\delta k_1 \to 0} \left| \frac{\mathrm{d}X_{\mathrm{E}}(k_1, r_2)\, \mathrm{d}X^*_{\mathrm{E}}(k_1, r_2)}{\delta k_1} \right|, \tag{4.2}$$

and analogously for $\phi(k_2)$. Aliasing of the one-dimensional spectrum was corrected by assuming that the prewhitened spectrum had a form $k_i^{-m+2}$. The value of $m$ was chosen to be 3 on the basis of the nominal exponent found for the one-dimensional wavenumber spectra. No aliasing correction was applied to the two-dimensional spectra. The above operations give a one-dimensional power spectrum with the property

$$\int_0^\infty \phi(k_1)\, \mathrm{d}k_1 = \overline{\eta'^2}, \tag{4.3}$$

where $\eta'$ is the elevation about the mean of each data line $\eta(r_1, r_2 = \text{constant})$ and the overbar implies the average over the lines of data which make up the frame. The prewhitening and anti-aliasing lead to the above relationship (4.3) being only approximately satisfied. Also, it should be noted that only in a stochastic sense (i.e. $n \to \infty$ in (4.1) and (4.2)) can the one-dimensional spectrum be shown to be equal to the integral of the two-dimensional spectrum.

While the absolute accuracy was estimated to be very close to 1 mm in elevation of the calibration target, the real limitation was the inability of the photogrammetrist to locate the ocean surface. Every tenth frame was re-read and the spectra of the differences of the duplicated data sets were calculated, maintaining identical Fourier processing including the anti-aliasing corrections (despite $m = 3$ being a poor approximation of the noise spectra). On the assumption that the reading errors are uncorrelated from reading one frame to the next, one half of the difference spectrum was used as an estimate of the noise floor for individual frames. The averaged one-dimensional spectra along the reading lines had a lower noise than those across the reading lines. This motivated the use of composite two-dimensional spectra averaged over the two reading directions.

If the data lines were statistically independent, each spectral estimate would have about 64 degrees of freedom (d.f.) and 95% confidence limits have been calculated on this basis. To examine the actual dependence of the data lines, a correlation analysis of the prewhitened height estimates was carried out for several frames. The probability distribution of the correlation coefficient between lines was examined and although it varied from frame to frame, it was found typically that pairs of data lines more than three data lines apart were consistent with the assumption of independence. Thus the 95% confidence limits would be somewhat wider than for 64 d.f. and would vary from frame to frame.

## 5. Results

The data forming the basis of this paper were taken as part of the BASS '84 and BASS X oceanographic experiments. The prevailing conditions are presented in tables 1 and 2 for the four experiments chosen for analysis. These experiments represented a good spread of wind speeds and wave ages. Experiment 1 had both the lowest wind speed and lowest significant steepness (defined as significant wave height divided by average wavelength). Experiment 2, with a much higher wind speed, exhibited the largest steepness among the four wave fields and visual observation

| Exp no. | Date | Wind speed ($ms^{-1}$) | Wind direction (from) | Air temp $T_a$ °C | Wet bulb temp. $T_w$ °C | Sea temp. SST °C | Significant wave height (m) | No. of frames used | Film roll no. |
|---|---|---|---|---|---|---|---|---|---|
| 1 | 26/2/84 | 7 | E | 24 | 17.0 | NA | 1.00 | 35 | 2 |
| 2 | 28/2/84 | 12 | SW | 15.5 | 11.3 | NA | 2.23 | 70 | 16 |
| 3 | 16/2/86 | 5.5 | E | 20.0 | 18.0 | 19.0 | 1.66 | 21 | 11 |
| 4 | 19/2/86 | 13.3 | W | 16.8 | 13.1 | 18.0 | 2.46 | 22 | 27 |

TABLE 1. Details of experiments

| Experiment number | Time (h) | Significant wave height (m) | Dominant wave period (s) |
|---|---|---|---|
| 1 | −3 | 1.05 | 8.13 |
| 1 | −2 | 1.07 | 7.53 |
| 1 | −1 | 1.01 | 6.48 |
| 1 | 0 | 1.00 | 5.75 |
| 2 | −3 | 2.57 | 5.33 |
| 2 | −2 | 2.56 | 5.51 |
| 2 | −1 | 2.37 | 5.12 |
| 2 | 0 | 2.23 | 4.88 |
| 3 | −3 | 1.59 | 6.48 |
| 3 | −2 | 1.67 | 6.65 |
| 3 | 1 | 1.62 | 6.74 |
| 3 | 0 | 1.66 | 6.56 |
| 4 | −3 | 2.56 | 5.51 |
| 4 | −2 | 2.73 | 5.57 |
| 4 | −1 | 2.58 | 5.63 |
| 4 | 0 | 2.46 | 5.45 |

TABLE 2. Details of wave conditions prior to the experiments

confirmed the occurrence of widespread white-capping. Since the wind was from the south west, through Bass Strait, the wave field did not have a large swell component. Experiment 3 was a situation where the wind had freshened before the measurements but the significant wave height had yet to respond. By way of contrast, preceding the measurements in experiment 4, the winds had been steady and the sea had risen to become steady a few hours earlier, as shown in table 2. The significant slope was almost twice as large in experiment 4 as in experiment 3 and the wave age $c/u_*$ was about half. The range of the key parameter $u_*^2 k/g$ covered by our experiments extended from $1.75 \times 10^{-3}$ to $100 \times 10^{-3}$.

To illustrate the technique, a typical photographic frame taken from experiment 2 is shown in figure 2(*a*). The corresponding topography determined by stereo-photogrammetric analysis is shown in the form of a similarly scaled contour plot in figure 2(*b*). In this figure, the background slope of the dominant wave is clearly evident. Removal of the background mean slope of this frame highlights the smaller-scale features of the topography, as seen in figure 2(*c*), which has half the contour interval as figure 2(*b*). It should be noted that the resolved small-scale topographic variations, i.e. those with wavelengths longer than 0.2 m, appear to have no

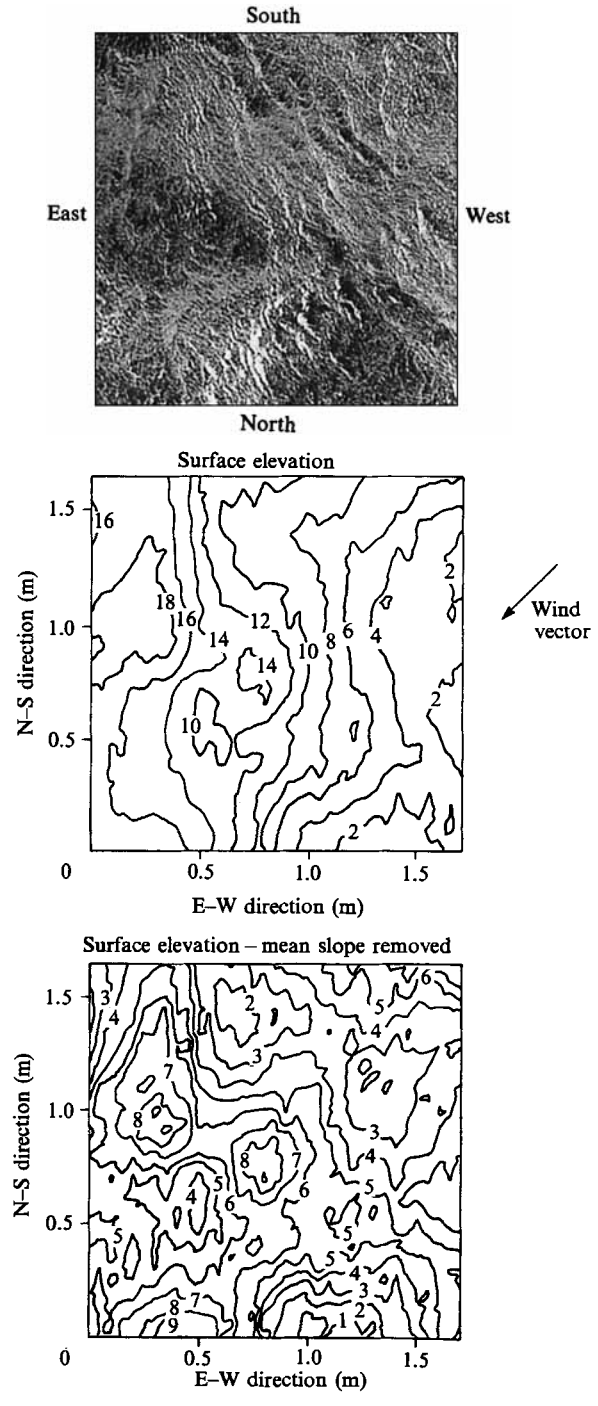


FIGURE 2. (*a*) Photograph of sea surface taken at $t = 4.5$ s during experiment 2. The field of view is approximately 1.6 m × 1.6 m. The mean windspeed was 12 m/s from the south west. (*b*) Similarly scaled contour plot of the sea surface topography determined stereophotogrammetrically from the images corresponding to (*a*). The contours shown indicate the relative height above a horizontal plane in 0.02 m increments. (*c*) Contour plot of (*b*) with the mean surface slope removed to reveal the small-scale variability. The contour height interval is 0.01 m.

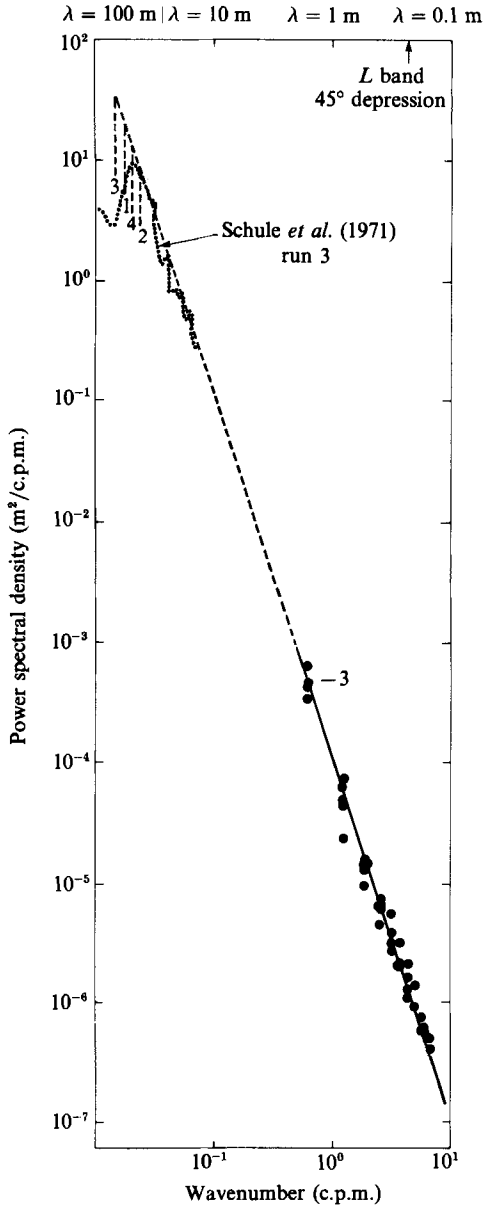


FIGURE 3. One-dimensional power spectral density in terms of wavenumber for all the experiments. Peak wavenumbers deduced from the wave period are shown coded by the experiment number.

preferred directions and, in particular, correlation with the wind direction is very low. The stereophotogrammetrically resolved components are underlying the (unresolved) finer scale structures most visible in the photograph of figure 2(*a*), which have much stronger visual correlation with the wind direction.

All the one-dimensional wavenumber spectra from a particular experiment were averaged together and corrected for noise and aliasing effects to produce the north–south and east–west wavenumber spectra presented in figure 3. The solid line shown in figure 3 has a power law dependence of $k_1^{-3}$ or $k_2^{-3}$ and this appears to be a reasonable approximation to the trend of all the data. This aspect is analysed in

considerable detail below. The directional nature of the spectra is considered subsequently. Included in figure 3 are longer wavelength results obtained by Schule, Simpson & De Leonibus (1971). These results, embracing the most energetic wave components appear to be well-described by $k_1^{-3}$. Also indicated in figure 3 is the spectral peak wavenumber for each experiment, calculated from the average zero-crossing period from the wave gauge signal on the assumption of the dispersion relation for free gravity waves.

Since we are sampling from a field with low wavenumber components much more energetic than the wavenumber band (0.63–5 cycles per metre (c.p.m.)) that was resolved by the digitized stereophotographs, we were concerned that our high wavenumber spectra should not be distorted by spurious leakage of low wavenumber energy, the most energetic of the latter having $10^4$ greater spectral density than at 0.63 c.p.m. as can be seen in figure 3. To verify that our prewhitening method effectively precluded such spectral leakage, a simulated one-dimensional spatial series with a known spectrum of $k^{-3}$ above the spectral peak was processed using our analysis program. The results showed that the output spectrum in our region of interest followed very closely the input $k^{-3}$ spectrum and was insensitive to the choice of the low wavenumber corresponding to the spectral peak. As the spectral processing of two-dimensional digital topographic data comprises a sequence of one-dimensional processing stages, it was inferred that our prewhitening technique satisfactorily reduced spurious low wavenumber leakage to negligible levels in the spectral analysis of the actual data.

On the basis of the discussions in §2, the data was used to determine the power law dependence of the 'saturation' (Phillips 1985), as expressed by the dependence of $k_i^3 \phi(k_i)$ on the parameter $u_*^2 k_i/g$ for $i = 1, 2$. The friction velocity was determined (after a suitable conversion of the anemometer height from 54 m to 10 m) using the relationship of Wu (1980) under the assumption of neutral conditions (the available atmospheric stability parameters are summarized in table 1).

Figure 4 shows the distribution of observed values of the saturation $k_i^3 \phi(k_i)$ versus $u_*^2 k_i/g$. The distribution of the saturation versus $u_*^2 k_i/g$ has been fitted by a power law relationship: a least-squares regression analysis was carried out for the logarithm of the saturation against the logarithm of $u_*^2 k_i/g$ to determine the coefficient $A$ and exponent $\gamma$ in

$$k_i^3 \phi(k_i) = A \left( \frac{u_*^2 k_i}{g} \right)^{\gamma}. \tag{5.1a}$$

Under the assumption that the logarithms of the saturation and $u_*^2 k_i g$ are normally distributed, the confidence levels were determined using the variances and covariances of the data about the regression line. This analysis gave

$$A = 1.52 \times 10^{-4}, \quad \gamma = 0.09 \pm 0.09, \tag{5.1b}$$

at the 95% confidence level.

As a lowest-order approximation to (5.1*b*), the wind-speed dependence might be neglected and our observed power law dependence for the one-dimensional wavenumber spectrum approximated at $(u_*^2 k_i/g) = 10^{-2}$ by

$$\phi(k_i) = 10^{-4} k_i^{-3} \quad (i = 1, 2), \tag{5.1c}$$

with the corresponding two-dimensional form

$$\psi(\boldsymbol{k}) = 0.3 \times 10^{-4} k^{-4}. \tag{5.1d}$$

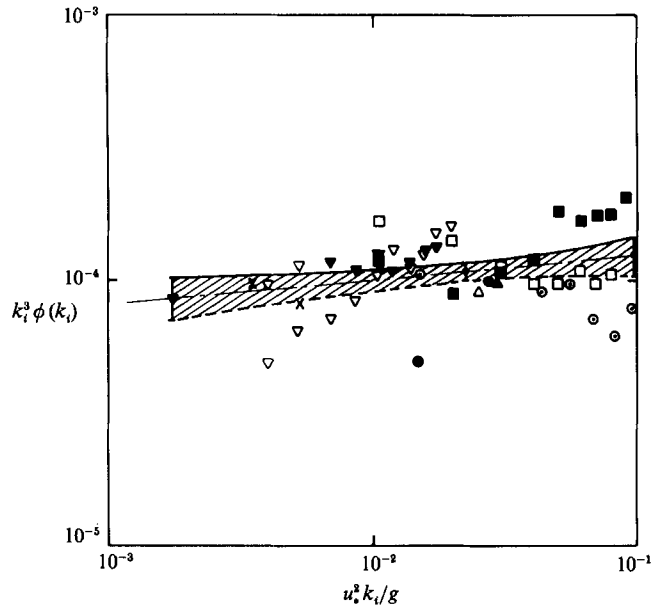


FIGURE 4. Saturation $k_i^3\phi(k_i)$ as a function of wavenumber $u_*^2 k_i/g$ for $i = 1$ (N–S) and $i = 2$ (E–W) for the various experiments. ×, Experiment 1 (N–S); +, experiment 1 (E–W); □, experiment 2 (N–S); ■, experiment 2 (E–W); ▼, experiment 3 (N–S); ▽, experiment 3 (E–W); ⊙, experiment 4 (N–S); ●, experiment 4 (E–W). The shaded region defines the 95% confidence limits.

The approximations (5.1*c*) and (5.1*d*) conform to the wavenumber dependence, when the value of the parameter $\gamma$ equals 0, of the one-dimensional equilibrium spectrum corresponding to (2.4) and the equivalent isotropic two-dimensional equilibrium spectrum (2.2), which represent a physical balance between nonlinear spectral transfer and dissipation and with a hard-limiting model (Phillips 1958). It is interesting to note that the recent equilibrium range models of Kitaigorodskii (1983) and Phillips (1985) propose

$$\phi(k_i) \sim u_* g^{-1/2} k_i^{-2.5} \quad (i = 1,2), \tag{5.2}$$

corresponding to $\gamma = 0.5$ in (2.2). Within the 95% confidence limits, there is no observational support for the linear dependence on $u_*$ implied by (5.2) in our wavenumber range. While relating the wind speed at 54 m to the surface friction velocity $u_*$ is not straightforward, the present results for wavenumber components in the range 0.63–5 c.p.m. are not supportive of the simple spectral balances envisaged by Kitaigorodskii (1983) or Phillips (1985). A more direct determination of the wind stress would be preferable in future studies, but only minor variations are to be expected from the established drag laws.

Although the number of photographs required for reliable modulation information greatly exceeds the number of images we processed, it is of some interest to examine the fluctuations in power spectral density of the average spectra of each 1.6 m × 1.6 m photographic region that constituted the experiment average in figure 3. The water elevation as the longer waves propagate past our observation point in experiment 2 is shown in figure 5 together with the one-dimensional directional spectral levels of wave components with 80 cm wavelengths. The mean over the experiment of power spectral density is shown at the right of each spectral history as well as the 95% confidence limits based on 64 d.f. Examining the modulation of

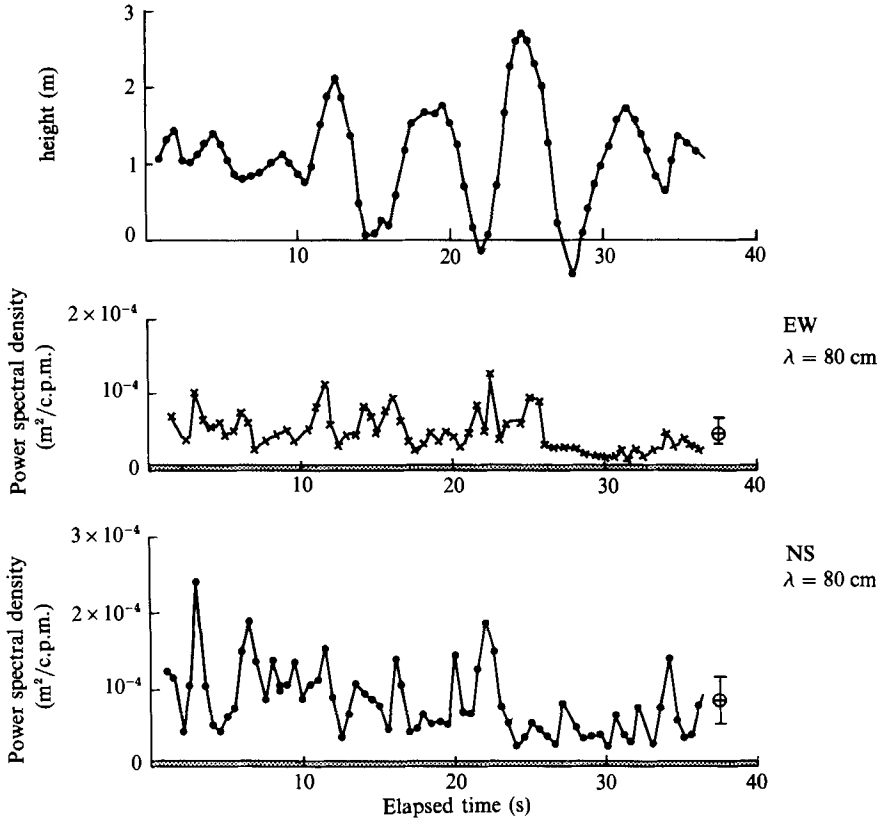


FIGURE 5. Time series of power spectral density of wavenumber components during an interval embracing a whitecapping event, uncorrected for noise. Wavelength = 0.80 m. Experiment 2. Water height is with respect to an arbitrary origin. Noise levels are shown for each wavenumber component as a shaded band. 95% confidence limits about the mean level are shown at the right.

the wave components in figure 5 for experiment 2, one sees evidence of fluctuations which exceed the confidence limits but these have little visual correlation with the underlying long wave. The only period in these figures where there appears to be a correspondence between the long-wave profile and the 0.80 m wavelength power spectral density where a number of sequential data points exceeds the confidence limits is around the elapsed time of 30 s. The photographs show that breaking of the long wave with whitecapping occurred on the crest that passed through the photographed region at 25 s elapsed time. Here the amplitudes of both directional components were reduced markedly. It appears that breaking leaves behind a region where the short waves are suppressed and that regeneration of the short-wave spectrum to pre-breaking levels is not complete by the end of the record, about two long-wave periods later, pointing to an enhanced persistence for the effects of whitecapping of the dominant waves in reducing the spectral levels of the short gravity-wave components. Depending on the extent of such whitecapping, this effect could well be important at higher windspeeds in contributing to an overall suppression of the short-wave spectrum at higher sea states, with a consequent lower $u_*$ spectral dependence.

The modulation of short waves by the characteristic long wave in wind-wave field

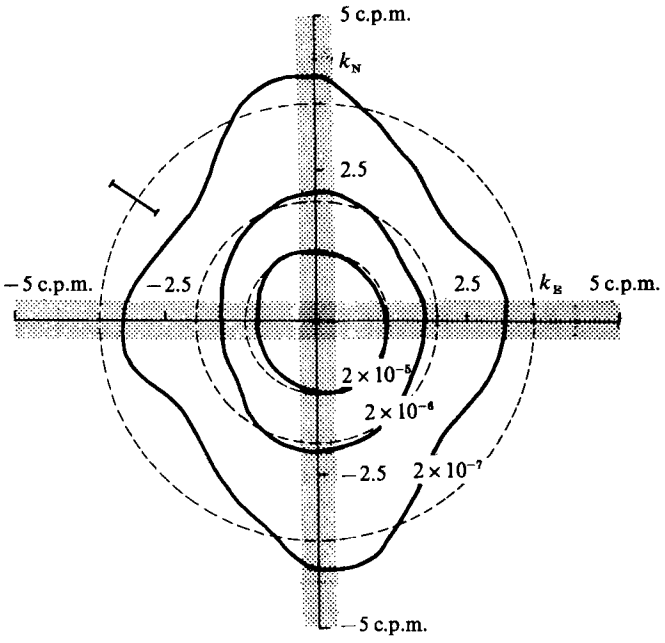


FIGURE 6. Two-dimensional power spectral density for experiment 3. Shaded area represents region where no estimate can be made. Confidence limits are for hypothetical spectra (see text). Superimposed contours are of $\psi(\boldsymbol{k}) = 0.3 \times 10^{-4}\, k^{-4}$. Units of spectral density are m²/c.p.m.².

is fundamental to an understanding of synthetic radar imaging of the ocean. However, with the apparent weak correlation evident here, a much longer ensemble of realizations would need to be analysed, an activity beyond the scope of the present contribution which must be left to the future as further processed image sequences become available.

Figures 6 and 7 show examples of two-dimensional wavenumber spectra, for experiments 3 and 4 respectively, uncorrected for noise.

The two-dimensional spectra show that for the short waves considered here, the distribution of energy is approximately equal in all directions, after taking into account the confidence limits. The two-dimensional spectra, computed from an ensemble of 14 photographic pairs, are assumed to have 28 d.f. and the confidence limits have been calculated for an assumed omni-directional spectrum with a wavenumber dependence $(k_1^2 + k_2^2)^{-2}$. Shown superimposed are contours of

$$\psi(\boldsymbol{k}) = 0.3 \times 10^{-4}\, k^{-4} \quad (k = |\boldsymbol{k}|), \tag{5.3}$$

representing the approximate fit (5.1 *d*) to the data. This $k^{-4}$ dependence is consistent with the observed one-dimensional wavenumber dependence. It should be noted that in this linear presentation, the confidence bands increase in width with increasing wavenumber. If the data series had been of much greater spatial extent there would have been a massive peak in the spectra near zero wavenumber. Details of the suppression of this unresolved contribution and the contributions along the wavenumber axes are described earlier in §4.

The two-dimensional spectra have a reflectional symmetry in wavenumber,

$$\text{i.e.} \quad \psi(\boldsymbol{k}) = \psi(-\boldsymbol{k})$$

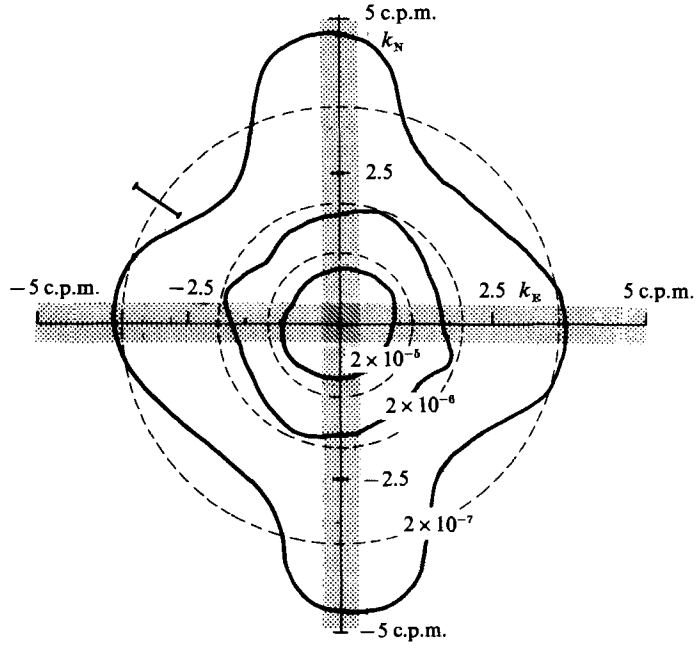


FIGURE 7. Two-dimensional power spectral density for experiment 4. Shaded area represents region where no estimate can be made. Confidence limits are for hypothetical spectra (see text). Superimposed contours are of $\psi(\boldsymbol{k}) = 0.3 \times 10^{-4} k^{-4}$. Units of spectral density are $m^2$/c.p.m.$^2$.

and therefore provide no information about the direction of propagation of the Fourier components. Frequency–wavenumber or phase velocity diagrams would be needed for this purpose. The lack of a preferred direction in the wavenumber spectra can be regarded as an indication of the short-crestedness of ocean surface gravity waves of the scale considered.

## 6. Discussion

This study provides for an improved awareness of the physical processes which underlie this high-wavenumber subrange of the ocean gravity-wave spectrum. The major results deriving from our measurements, which span the nominal wavelength range of 0.2–1.6 m, are as follows:

(*a*) For our spectral range, the observed spectral forms (5.1*a*,*b*) follow the equilibrium form proposed originally by Phillips (1958) rather than the recently revised forms due to Kitaigorodskii (1983) and Phillips (1985). These forms may be applicable within other spectral ranges.

(*b*) The findings in (*a*) are generally consistent with the lack of windspeed dependence, particularly with respect to wind direction, evident in the backscattered microwave power levels observed at longer microwavelengths (e.g. the *P*-band (0.7 m wavelength) and *L*-band (0.25 m wavelength) data of Guinard, Ransone & Daley (1971) and the more recent study of Thompson, Weissman & Gonzalez (1983)). At *P*-band, no trend with windspeed was reported, while a rather weak windspeed dependence exponent of 0.5 has been found for *L*-band radar backscatter. This is slightly stronger than our observed average wavenumber spectral dependence on the wind (within the 95% confidence limits, a windspeed exponent of up to 0.36 is possible for the average $u_*$ dependence of the wavenumber spectrum within our

wavelength range). At the shorter scales within our observation range the increased spectral levels suggest the possibility of a stronger windspeed dependence entering but it is felt that the signal-to-noise ratio for the present data precludes drawing this conclusion with any confidence. We are hopeful of extending our resolved spectral range to higher wavenumbers in a future extension of this research.

(*c*) From the observed wavenumber spectral form, it is of interest to estimate the contribution to the mean-squared slope from this spectral subrange. Defining this quantity in the usual way, as

$$\overline{(\nabla\xi)^2} = \overline{\xi_x^2} + \overline{\xi_y^2},$$

where $z = \xi(x, y, t)$ specifies the ocean surface and the overbar denotes a suitable average, it is easily established that, when the wavenumber is expressed in cycles/m,

$$\overline{(\nabla\xi)^2} = \iint 4\pi^2 k_1^2 \psi(k_1, k_2)\,\mathrm{d}k_2\,\mathrm{d}k_1 + \iint 4\pi^2 k_2^2 \psi(k_1, k_2)\,\mathrm{d}k_2\,\mathrm{d}k_1 = \iint 4\pi^2 k^2 \psi(\boldsymbol{k})\,\mathrm{d}k,$$

where

$$k = |\boldsymbol{k}|.$$

Using the observed form for $\psi(\boldsymbol{k})$ as specified in (5.3) above, it is found that the contribution to $\overline{(\nabla\xi)^2}$ from wavenumber magnitudes between $k_L$ and $k_U$ is

$$0.8 \times 10^{-2} \ln(k_U/k_L).$$

Setting $k_L = 1/1.6$ and $k_U = 1/0.2$, the mean squared slope contribution from our observed wavenumber range is 0.016. Based on the measurements of Cox & Munk (1954) and Tang & Shemdin (1983), our observed wavenumber range contributes a significant fraction of the total mean-squared slope. The average r.m.s. wave slope for this subrange is 7.3°, comparable with that of the region with wavelengths longer than 1.6 m and embracing the spectral peak. The observed finite slopes imply that nonlinear spectral transfers are unlikely to be negligible for this spectral region.

(*d*) From the observed weak dependence of the spectra on the wind strength, it would appear that the wind input is of secondary importance in determining the form of the spectrum for these scales. This is strengthened by the observed insensitivity of the spectra on the wind direction: the commonly assumed wind input source function is directional, (varying as the cosine of the angle between the wind vector and the wavenumber vector (see Snyder *et al.* 1981; Phillips 1985). The lack of observed dependence on the wind speed or direction and the non-directional spectral form suggests the importance of nonlinear spectral transfers which produce a significant directional redistribution of energy in wavenumber space, an effect which is enhanced with increasing wavenumber (Webb 1978; Hasselmann & Hasselmann 1985). However, this asymptotic high-wavenumber region of the gravity wave spectrum is well away from the usual focus of attention of the nonlinear wave–wave interaction calculations published in the literature, which have concentrated on the spectral region around the spectral peak. An exception is Hasselmann (1963, §4) in which asymptotic forms of the nonlinear 4-component interaction transfer rate are discussed briefly. Hasselmann concludes that, for the asymptotic $k^{-4}$ spectrum associated with a fully-developed Pierson–Moskowitz spectrum, the energy transfer is predominantly local in wavenumber space. However, the magnitudes of the asymptotic nonlinear transfer rates are not given so that comparison with estimated wind input transfer rates is not readily made. Also, no details on the asymptotic directional spreading characteristics are provided.

(*e*) Theoretical predictions for the asymptotic high-wavenumber subrange which

embraces our data have been based largely on postulated dynamic balances and functional forms derived on the basis of dimensional and order of magnitude arguments. Referring back to the discussion on possible dynamical balances it is evident that Phillip's (1958) prediction appears to fit our findings, though we are unable to verify directly its underlying assumptions of hard-limiting by wave-breaking (see §2). Indeed, it is unclear how this concept would lead to the observed broadly directional spectral distribution. For our observed wavenumber range, a balance involving nonlinear wave–wave interactions and dissipation predicts a spectral dependence consistent with our observations (see §2(*a*)), with wind input to these scales assuming a subordinate role.

It is indeed fascinating to note that at scales significantly shorter and longer than our observed range, the wave components appear visually to be more closely aligned with the wind direction and presumably are coupled to the wind more directly. The strength of the wind coupling near the spectral peak has been reported by Snyder *et al.* (1981) and by Hasselmann *et al.* (1986) and its strong influences on the evolution of the spectral peak region has been demonstrated by Komen *et al.* (1984). The strength of the wind coupling to the very shortest scales (typically 50–100 mm wavelengths) is clearly apparent through visual inspection (e.g. see figure 2(*a*)). This apparent variability in the underlying dominant spectral balance indeed makes this a phenomenon of considerable theoretical challenge. These observations also relate to the typical aerodynamic roughness lengths in the marine boundary layer, which point to roughness elements very much smaller than the heights of the waves in our observation range as well as the dominant waves. On the other hand, strong wind input is believed to occur near the peak of the ocean wave spectrum (e.g. Snyder *et al.* 1981; Komen *et al.* 1984). This suggests a two-scale wind input mechanism where significant wind input occurs at the dominant and very short wave scales, with the intermediate scales sheltered from direct contribution to the drag.

(*f*) The relationship of the present wavenumber observations to the more usually quoted frequency spectrum is also worth noting. Again, the majority of the reported frequency spectra for open ocean conditions are limited to three to four times the spectral peak frequency $\omega_p$ (e.g. Donelan *et al.* 1985). The published spectra which extend to $10\omega_p$ are reported as showing a significant dependence on the windspeed or friction velocity. The difficulties in relating such frequency spectra, known to be affected by Doppler shifting due to the underlying orbital motions of longer waves (and underlying mean currents), to the wavenumber spectrum have been explored in detail by several authors as described earlier in §2. Here we report on the form of the fixed frame frequency spectrum which might result from our observed wavenumber results. A straightforward calculation in the spirit of Kitaigorodskii *et al.* (1975) suffices to indicate the likely strength of the Doppler distortion effect: a more precise assessment would require knowledge of the wavenumber spectrum at higher wavenumbers than have been observed here. Figure 8 shows the result of transforming our observed wavenumber spectral form over the range $3\omega_p$ to $22\omega_p$. This calculation ignores spectral contributions from outside this range. It is evident that with increasing slope of the dominant wave, the net Doppler distortion produces a notable reduction in the slope of the tail of the spectrum and an increase in its energy level. For modest long-wave slopes $AK$ of 0.1, the slope of the tail has already increased from $-5$ to $-4$: higher long-wave steepness extends this effect dramatically. Under representative open ocean conditions, $AK \sim 0.1$, corresponding to a significant wave slope $H_s k_s/2\pi$ of about 0.03: under stronger generating situations, values of $AK$ up to 0.2 are appropriate. Thus this calculation serves to

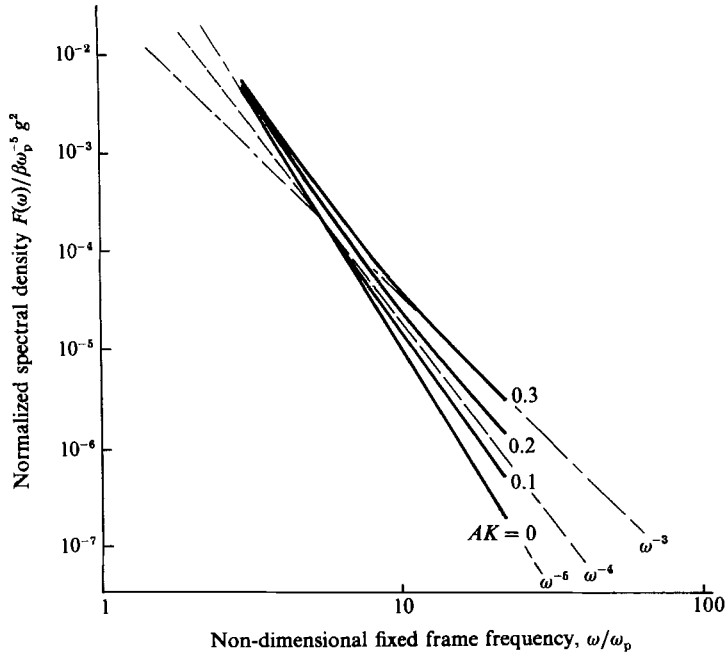


FIGURE 8. Computed normalized frequency spectra as a function of the dominant waveslope $AK$ for a two-dimensional short-wavenumber spectrum of the form given by equation (7.2). The effects shown are entirely the result of kinematic Doppler distortion. $\beta$ is the Phillips constant.

highlight the fact that a significant component of what is apparently a direct dynamical wind-speed dependence of the asymptotic high-frequency region of the frequency spectrum is likely to be due to the kinematic consequences of Doppler distortion due to underlying wave components at the peak of the spectrum. A contribution to the wind-speed dependence for this asymptotic region would occur through changes in the dominant wave slope, induced by the wind in combination with the other source terms, as discussed by Komen *et al.* (1984).

## 7. Conclusions

In the observed spectral range of 0.2–1.6 m wavelengths, our measurements support an equilibrium spectrum, with wavenumber in c.p.m., of the form

$$\phi(k_i) = 1.5\times10^{-4}\left(\frac{u_*^2 k_i}{g}\right)^{\gamma} k_i^{-3}, \tag{7.1}$$

where $\gamma = 0.09\pm0.09$ and $i = 1, 2$. That is, a wavenumber exponent of close to $-3$ and with a very weak dependence on the wind magnitude and direction. Our one- and two-dimensional spectra can be approximated respectively in this spectral range by the wind-independent forms, applicable for $(u_*^2 k/g) = 10^{-2}$, by

$$\phi(k_i) \sim 10^{-4} k_i^{-3}, \quad \psi(\boldsymbol{k}) \sim 0.3\times10^{-4} k^{-4} \quad (k = |\boldsymbol{k}|). \tag{7.2a,b}$$

It is noteworthy that when transformed to radian wavenumber units, the magnitude of the coefficient in (7.2*a*) is in close agreement with those cited for longer waves in

table 4.2 in Phillips (1977*a*), while that in (7.2*b*) closely matches the two-dimensional wavenumber spectral coefficient also reported in this table derived from the sea surface slope measurements of Cox & Munk (1954).

The form of these spectra imply that the steepest wave components within the range of gravity waves are those near the peak of the spectrum, rather than the very short gravity-wave components: this is consistent with the findings of Tang & Shemdin (1983). However, the components in our observed spectral range were estimated to make a significant contribution to the mean squared slope.

These results point to the importance of nonlinear spectral transfers in this short gravity-wave spectral subrange, with a reduced role for wind input in the equilibrium energy or action balance. However, detailed nonlinear wave interaction computations (e.g. Hasselmann 1963) have not been extended into this asymptotic high-wavenumber regime so that theoretical support for their relative strength is not yet available. Equilibrium spectral forms deduced from recently proposed physical models (Kitaigorodskii 1983; Phillips 1985) are found not to conform to our reported spectra within our observed wavenumber range.

On a local basis, the sudden reduction in amplitude of the short waves in the wake of a breaking event in the dominant wave field also points to a role for steep dominant waves in influencing the spectral levels of the short waves in a more complex manner than envisaged by the weakly nonlinear interaction models. This breaking episode provides an interesting example of how a short-wavenumber spectral region can be influenced strongly by events at much lower wavenumbers. The need to include such non-local interaction in the spectrum in the dissipation source term requires further study. The occurrence of such intermittent breaking events would be expected to increase with windspeed: their average contribution over larger spatial and temporal extents remains to be assessed. This also relates to the likely enhancement of radar returns from spilling breakers (Valenzuela 1985), which could account for the observed increase in $L$-band radar backscatter with increasing windspeed.

When compared with radar backscatter observed from the sea surface under assumed Bragg resonant conditions, our spectra reveal comparable insensitivity to the wind direction. Though generally insensitive to the windspeed over most of our observed wavenumber range, published radar return measurements at the shortest wavelengths in this range show a somewhat stronger (though still relatively weak) windspeed dependence. An extension of our observations to higher wavenumbers is needed to examine this aspect in greater detail.

Further study of the high-wavenumber region of the ocean wavenumber spectrum is needed to resolve the fundamental issues raised by this investigation: it is envisaged that future efforts will resolve higher-wavenumber components and will address the question of short-wave modulation by the underlying longer-wave components.

We wish to thank ESSO–BHP for allowing us to make measurements over a number of years from their Bass Strait platforms. Also we gratefully acknowledge the financial support of the Australian Marine Science and Techology (MST) Grants Scheme, an important contribution towards the success of this project.

## REFERENCES

ATAKTURK, S. S. & KATSAROS, K. B. 1987 Intrinsic frequency spectra of short capillary-gravity waves obtained from temporal measurements of wave height on a lake. *J. Geophys. Res.* **92**, 5131–5141.

COX, C. S. & MUNK, W. H. 1954 Statistics of the sea surface derived from sun glitter. *J. Marine Res.* **13**, 198–227.

DOBSON, E. B. 1970 Measurement of the fine-scale structure of the sea. *J. Geophys. Res.* **75**, 2853–2856.

DONELAN, M. A., HAMILTON, J. & HUI, W. H. 1985 Directional spectra of wind-generated waves. *Phil. Trans. R. Soc. Lond.* A **319**, 509–562.

EVANS, D. D. & SHEMDIN, O. H. 1980 An investigation of the modulation of capillary and short gravity in the open ocean. *J. Geophys. Res.* **85**, 5019–5024.

FORRISTALL, G. K. 1981 Measurements of a saturated range in ocean wave spectra. *J. Geophys. Res.* **86**, 8075–8084.

GOTWOLS, B. L. & IRANI, G. B. 1980 Optical determination of the phase velocity of short gravity waves. *J. Geophys. Res.* **85**, 3964–3970.

GUINARD, N. W., RANSONE, J. T. & DALEY, J. C. 1971 Variation of the NRCS of the sea with increasing roughness. *J. Geophys. Res.* **76**, 1525–1538.

HASSELMANN, K. 1963 On the non-linear energy transfer in a gravity-wave spectrum. Part 3. Computation of the energy flux and swell-sea interaction for a Neumann spectrum. *J. Fluid Mech.* **15**, 385–398.

HASSELMANN, K. 1974 On the spectral dissipation of ocean waves due to white capping. *Boundary-Layer Met.* **6**, 107–127.

HASSELMANN, D., BOSENBERG, J., DUNCKEL, M., RICHTER, K., GRUNEWALD, M. & CARLSON, H. 1986 Measurements of wave-induced pressure over surface gravity waves. In *Wave Dynamics and Radio Probing of the Sea Surface* (Ed. O. M. Phillips & K. Hasselmann), pp. 353–368. Plenum.

HASSELMANN, S. & HASSELMANN, K. 1985 Computations and parameterizations of the nonlinear energy transfer in a gravity-wave spectrum. Part 1. A new method for efficient computations of the exact nonlinear transfer integral. *J. Phys. Oceanogr.* **15**, 1369–1377.

HOLTHUIJSEN, L. H. 1983 Stereophotography of ocean waves. *Appl. Ocean Res.* **5**, 204–209.

KAHMA, K. K. 1981 A study of the growth of the wave spectrum with fetch. *J. Phys. Oceanogr.* **11**, 1503–1515.

KARARA, H. M. & ABDEL-AZIZ, Y. I. 1974 Accuracy aspects of non-metric imageries. *Photogrammetric Engng* **40**, 1107–1117.

KAWAI, S., OKUDA, K. & TOBA, Y. 1977 Field data support of three-seconds power law and $gu_* \sigma^{-4}$ spectral form for growing wind waves. *J. Oceanogr. Soc. Japan* **33**, 137–150.

KITAIGORODSKII, S. A. 1983 On the theory of the equilibrium range in the spectrum of wind-generated gravity waves. *J. Phys. Oceanogr.* **13**, 816–827.

KITAIGORODSKII, S. A., KRASITSKII, V. P. & ZASLAVSKII, M. M. 1975 On Phillips' theory of equilibrium range in the spectra of wind-generated gravity waves. *J. Phys. Oceanogr.* **5**, 410–420.

KOMEN, G. J., HASSELMANN, S. & HASSELMANN, K. 1984 On the existence of a fully developed wind-sea spectrum. *J. Phys. Oceanogr.* **14**, 1271–1285.

KONDO, J., FUJINAWA, Y. & NAITO, G. 1972 Wave induced wind fluctuations over the sea. *J. Fluid Mech.* **51**, 751–771.

LUBARD, S. C., KRIMMEL, J. E., THEBAUD, L. R., EVANS, D. D. & SHEMDIN, O. H. 1980 Optical image and laser slope meter intercomparisons of high frequency waves. *J. Geophys. Res.* **85**, 4957–4966.

MITSUYASU, H. 1977 Measurement of the high frequency spectrum of ocean surface waves. *J. Phys. Oceanogr* **7**, 882–891.

PHILLIPS, O. M. 1958 The equilibrium range in the spectrum of wind-generated waves. *J. Fluid Mech.* **4**, 426–434.

PHILLIPS, O. M. 1977*a* *The Dynamics of the Upper Ocean.* Cambridge University Press, 336 pp.

PHILLIPS, O. M. 1977*b* The sea surface. In *Modelling and Prediction of the Upper Layers of the Ocean* (ed. E. B. Kraus, pp. 229–237. Pergamon.

PHILLIPS, O. M. 1985 Spectral and statistical properties of the equilibrium range in wind-generated gravity waves. *J. Fluid Mech.* **156**, 505–531.

PIERSON, W. J. (ed.) 1962 The directional spectrum of a wind generated sea as determined from data obtained by the Stereo Wave Observation Project. *Coll. Engng, N.Y.U. Met.* Pap. 2, no. 6.

RICHTER, K. & ROSENTHAL, W. 1986 Energy distribution of waves above 1 Hz on long wind waves. In *Wave Dynamics and Radio Probing of the Sea Surface* (ed. O. M. Phillips & K. Hasselmann), pp. 75–94. Plenum.

SCHULE, J. J., SIMPSON, L. S. & DE LEONIBUS, P. S. 1971 A study of fetch limited wave spectra with an airborne laser. *J. Geophys. Res.* **76**, 4160–4171.

SNYDER, R. L., DOBSON, F. W., ELLIOTT, J. A. & LONG, R. B. 1981 Array measurements of atmospheric pressure fluctuations above surface gravity waves. *J. Fluid Mech.* **102**, 1–59.

STILLWELL, D. 1969 Directional energy spectra of the sea from photographs. *J. Geophys. Res.* **74**, 1974–1986.

STILLWELL, D. & PILON, R. O. 1974 Directional spectra of surface waves from photographs. *J. Geophys. Res.* **79**, 1277–1285.

STOLTE, S. 1984 Modulation of short waves by long wind waves and wind. PhD Dissertation. University of Hamburg. 199pp.

SUGIMORI, Y. 1975 A study of application of the holographic method to the determination of the directional spectrum of ocean waves. *Deep-Sea Res.* **22**, 339–350.

TANG, S. & SHEMDIN, O. H. 1983 Measurement of high frequency waves using a wave follower. *J. Geophys. Res.* **88**, 9832–9840.

THOMPSON, T. W., WEISSMAN, D. E. & GONZALEZ, F. I. 1983 L band radar backscatter dependence upon surface wind stress: a summary of new SEASAT-1 and aircraft observations. *J. Geophys. Res.* **88**, 1727–1735.

TOBA, Y. 1973 Local balance in the air–sea boundary processes, III. On the spectrum of wind waves. *J. Oceanogr. Soc. Japan* **29**, 209–220.

VALENZUELA, G. R. 1985 Microwave sensing of the sea surface. In *The Ocean Surface: Wave breaking, Turbulent Mixing and Radio Probing* (ed. Y. Toba & H. Mitsuyasu), pp. 233–244. Reidel.

WEBB, D. J. 1978 Nonlinear transfers between sea waves. *Deep-Sea Res.* **25**, 279–298.

WILLS, J. A. B. 1984 Model tests on the Noordwijk tower. *Rep.* R184, NMI, Ltd. Feltham, Middlesex, UK.

WU, J. 1980 Wind-stress coefficients over sea surface near neutral conditions – a revisit. *J. Phys. Oceanogr.* **10**, 727–740.